Original paper

Cymrite, celsian and associating Ba-rich minerals in metacarbonates from the Čučma – Čierna baňa manganese deposit (Slovakia, Western Carpathians)

Pavol MYŠĽAN1*, Peter RUŽIČKA2, Martin ŠTEVKO1,3, Tomáš MIKUŠ4

- ¹ Earth Science Institute, Slovak Academy of Sciences, Dúbravská cesta 9, 840 05 Bratislava, Slovakia; pavol.myslan@sayba.sk
- ² Department of Mineralogy, Petrology and Economic Geology, Faculty of Natural Sciences, Comenius University, Ilkovičova 6, 842 15, Bratislava, Slovakia
- ³ Department of Mineralogy and Petrology, National Museum, Cirkusová 1740, 193 00 Prague 9-Horní Počernice, Czech Republic
- ⁴ Earth Science Institute, Slovak Academy of Sciences, Ďumbierska 1, 974 11 Banská Bystrica, Slovakia
- *Corresponding author



The Čučma - Čierna baňa manganese deposit (Slovakia, Western Carpathians) hosts barium-rich mineralisation within the Early Paleozoic metacarbonate lenses associated with graphite-, quartz-muscovite phyllites and metalydites. The main metacarbonate mineral is represented by calcite containing up to 94.2 mol. % CaCO,, with minor amounts of Mn, Fe and Mg constituents. The Ba-mineralisation consists of silicates such as cymrite, celsian, Ba-rich muscovite and baryte along with clinochlore, quartz, spessartine and accessory fluorapatite and rutile. Cymrite forms prismatic to tabular aggregates, commonly associated with celsian and Ba-rich muscovite, it displays a stable chemical composition close to the theoretical end-member formula. Celsian (89.0-97.3 mol. % Cls) with minor Na, K, Ca, and Sr contents typically occurs as anhedral grains and is overgrown by cymrite, indicating a possible hydration transformation. Ba-rich muscovite shows complex chemical zoning, suggesting variable Ba incorporation through multiple substitutions predominantly in Ba-enriched zones (up to 0.32 apfu Ba). Clinochlore lacks any Ba and is interpreted as a retrograde phase. Textural, chemical and structural evidence studied by optical microscopy, electron microprobe analyses (EPMA) and Raman spectroscopy indicates a multi-stage development involving baryte or barium enrichment during sedimentation influenced by submarine basic volcanism, subsequently followed by Variscan and Alpine metamorphic events. Metamorphic recrystallisation mobilised Ba, leading to the formation of Ba-rich silicates. The Ba-rich mineral assemblage and associated textures reflect the complex metamorphic evolution of the deposit and highlight cymrite and celsian as a key indicator of low-grade metamorphism in the studied Ba-rich environment. The presence of spessartine (up to 60.0 mol. % Sps) and other accessory phases further illustrates a close relation with associated manganese mineralisation.

Keywords: cymrite, celsian, Ba-rich muscovite, metacarbonates, Čučma, Slovakia Received: 2 July 2025; accepted: 17 September 2025; handling editor: J. Sejkora The online version of this article (doi: 10.3190/jgeosci.0032.25) contains electronic supplementary material.

1. Introduction

Barium is generally present as a minor component in silicate minerals, however it can become significantly enriched in specific environmental settings as Ba-rich mineralisations occur within different types of ore deposits (e.g. Essene et al. 2005; Raith et al. 2014; Chang et al. 2018; Bermanec et al. 2023). In manganese and ferromanganese deposits, such enrichment has been reported from several locations, including the Jhabua manganese belt in India (Das Gupta et al. 1970), the iron-manganese-barium deposit in the Afar Rift, Ethiopia (Bonatti et al. 1972), Mn-rich rocks on Andros Island, Greece (Reinecke 1982), the calcite-dolomite Franklin Marbles of Sterling Hill, New Jersey (Tracy 1991), Mn-rich iron formations of the Cuyuna Iron Range, Minnesota

(McSwiggen et al. 1994), the Shiromaru Mn deposit in Japan (Matsubara et al. 2000), metamorphosed manganoan marbles from Pittsylvania County, Virginia (Tracy, Beard 2003), the Bistrita manganese belt in Romania (Hirtopanu et al. 2008), the Benallt manganese mine in Wales (Cotterell 2012), the Postmasburg manganese field, South Africa (Costin et al. 2015), pyrite and manganese ore deposit Chvaletice (Sejkora et al. 2025) or manganese deposit Kojetice near Třebíč (Novák and Škoda 2007) Czech Republic, and many others.

Barium-bearing minerals, such as cymrite (BaAl₂Si₂O₈·H₂O), celsian (BaAl₂Si₂O₈) Ba-rich muscovite [(K_{1-x},Ba_x)Al₂(Al_{1+x}Si_{3-x}O₁₀)(OH)₂] and baryte (BaSO₄) serve as essential index minerals of certain geochemical and metamorphic conditions in Ba-enriched manganese-bearing deposits mostly occurring

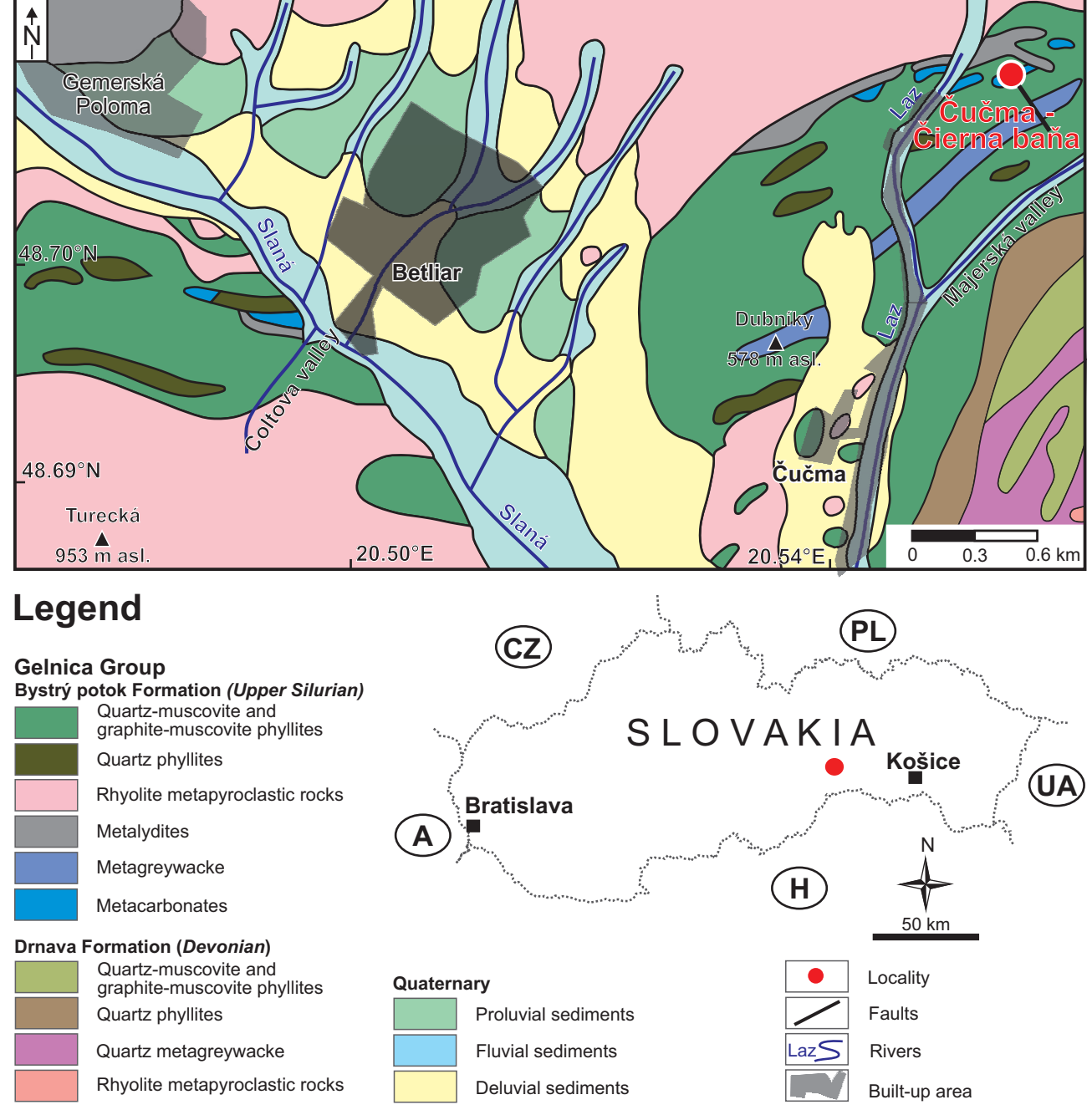


Fig. 1 Geological map of the Betliar-Čučma area with occurrence of Ba-rich mineralisation hosted in metacarbonates at the locality Čučma – Čierna baňa in the Spišsko-gemerské rudohorie Mts. (modified after Bajaník et al. 1983).

with quartz, carbonates, *hyalophane*, albite and apatite (Sorokhtina et al. 2008). These minerals typically form in metasedimentary, hydrothermal or metasomatic environments and are associated with low-, medium- to high-grade metamorphism (Green et al. 2019; Matsubara et al. 2000; Moro et al. 2001). Their coexistence is an important indicator of Ba activity in the metamorphic systems (Sorokhtina et al. 2008).

All major occurrences of metamorphosed manganese mineralisation in Spišsko-gemerské rudohorie Mts.

have been studied recently (Radvanec and Gonda 2020; Myšľan et al. 2023, 2024, 2025a, b and others mentioned below), but no evidence of Ba-rich minerals (except baryte) was found in Mn ore, nor associated rocks. Therefore, this study presents the first occurrence of cymrite, celsian, Ba-rich muscovite and associating minerals from Čučma – Čierna baňa manganese deposit in Slovakia, discusses their mineralogical and textural characteristics and evaluates their implications for the metamorphic evolution and fluid history of the host metacarbonate rocks.

2. Geological settings and localisation

The Gemeric Unit is composed of Lower Paleozoic basement (Gelnica and Rakovec Group), Upper Paleozoic (Ochtiná, Dobšiná and Gočaltovo Group) and Lower Triassic (Kobeliarovo Group) cover complexes (Bajaník et al. 1983). The Lower Paleozoic Gemeric basement units are interpreted to have evolved as riftogenic zones associated with Gondwana active margin (Grecula 1982; Putiš et al. 2008). The studied area of metacarbonate occurrence with Ba-rich mineralisation belongs from the lithostratigraphic point of view to the Gelnica Group, which is represented by polygenetic and polycyclic formations that retain flysch-like features of its original sedimentation basin, accompanied by synchronous acid and basic volcanism. These sequences consist of cyclically arranged metapsammites and metapelites associated with meta-volcanoclastic material. The Gelnica Group is subdivided into the Vlachovo, Bystrý potok, and Drnava Formations. Studied metacarbonate lenses occur locally in the upper parts of Bystrý potok Formation associated with metalydites and phyllites (Bajaník et al. 1983; Vozárová 1993). Crystalline limestone's appearance is a result of boudinage formed during Variscan metamorphism and subsequently deformed during the development of the Alpine nappe-fold structure (Grecula et al. 1995).

The age of the Gelnica Group is constrained to the Late Cambrian–Early Devonian, based on biostratigraphy and geochronology (Snopková, Snopko 1979; Soták et al. 2000). Volcanic events in the Southern Gemericum peaked during the Furongian (~492 Ma), Tremadocian (~481 Ma), and Darriwilian (~464 Ma) stages prolonged into late Ordovician in the Bystrý potok Formation as confirmed by U-Pb SHRIMP dating of zircons from rhyolitic metavolcanoclastics (Vozárová et al. 2017). The Bystrý potok Formation yielded zircon ages of 465.8 ± 1.5 Ma (Vozárová et al. 2010). The structure of the Gelnica Group has a banded appearance due to Variscan and Alpine folding and metamorphism, however despite Alpine reworking, features of the Variscan metamorphism remain preserved (Grecula et al. 1995). The Gelnica Group underwent regional metamorphism under greenschist facies conditions (Faryad 1991, 1995; Vozárová 1993) estimated at 350–370 °C and 300–500 MPa (Sassi, Vozárová 1987; Mazzoli, Vozárová 1989).

Metamorphic manganese mineralisation is closely associated with lenses of metacarbonates containing Ba-rich mineralisation (Fig. 1), which is the subject to this detailed mineralogical research. The Čierna baňa manganese deposit is located on the western slope of Stredná hora hill, near the northern edge of Čučma village, approximately 6 km NE of Rožňava. The polygenetic Mn mineralisation forms lens-shaped bodies (Rojkovič 2001). The ore bodies are 50–100 m long, 1–4 m thick, dipping

50–60° southward (Grecula et al. 1995). Mining of the deposit targeting mostly the supergene zone was active from the late 19th to early 20th century (Grecula et al. 1995). Originally a stratiform sedimentary Mn deposit was later overprinted by Variscan metamorphism under conditions at 375–420°C under 350 MPa (Faryad 1994; Rojkovič 1999). The mineral composition of the individual phases forming the primary and secondary mineral association has been studied by several authors, who have identified more than 80 minerals (Faryad 1994; Faryad, Zábranský 1996; Rojkovič 1999, 2000, 2001; Peterec, Ďuďa 2003, 2009; Števko et al. 2015; Radvanec and Gonda 2020). Samples of metacarbonates with Ba-rich mineralisation were collected at the old dumps at the following GPS coordinates: 48°42'32"N 20°32'57"E (WGS84).

3. Analytical methods

The representative samples of metacarbonates were processed into the multiple polished thin sections from which only CU-8, CU-13 and CU-15 contained Ba-rich mineralisation selected for further study using a polarised optical microscope Leica DM2500P (Department of Mineralogy, Petrology and Economic Geology, Faculty of Natural Sciences, Comenius University, Bratislava).

Quantitative chemical (WDS) analyses of studied minerals were obtained using a JEOL-JXA850F fieldemission electron microprobe (EMPA) in wavelengthdispersive spectrometry (WDS) mode (Earth Science Institute, Slovak Academy of Sciences, Banská Bystrica, Slovakia). The following conditions were applied: accelerating voltage 15 kV, beam current 20 nA (silicates, carbonates and sulfates), counting time 20 s for peak and 10 s for background. The beam diameter ranged from 5 to 10 μm, ZAF correction was used. The following standards and X-ray lines were used: albite (Al $K\alpha$, Na $K\alpha$), baryte (SK α , BaL α), celestine (SrL α), Cr₂O₂ (CrK α), diopside (Si $K\alpha$, Mg $K\alpha$, Ca $K\alpha$), apatite (P $K\alpha$), fluorite $(FK\alpha)$, gahnite $(ZnK\alpha)$, hematite $(FeK\alpha)$, orthoclase $(KK\alpha)$, rhodonite $(MnK\alpha)$, rutile $(TiK\alpha)$, ScVO₄ $(VK\alpha)$, tugtupite (Cl $K\alpha$) and YPO₄ (Y $L\alpha$). In fluorapatite were further measured: CePO₄ (CeLα), LaPO₄ (LaLα), NdPO₄ $(NdL\alpha)$, $PrPO_4$ $(PrL\beta)$, $SmPO_4$ $(SmL\beta)$, ThO_5 $(ThM\alpha)$ and in rutile: cassiterite (SnL α), LiNbO₃ (NbL $\bar{\alpha}$), scheelite $(WM\alpha)$, ZrO_{α} $(ZrL\alpha)$. The detection limit of each element ranged from 0.005-0.030 wt. %. Elements that were analysed quantitatively and are below the detection limit are not listed in the tables. Analytical protocols are listed together with all chemical analyses in the Electronic Supplementary Material (ESM1). Photographic documentation of relationships between minerals was carried out in the BSE mode. Abbreviations of minerals are defined in Warr (2021).

The Raman spectra of selected minerals were acquired using a Thermo Scientific DXR3xi Raman Imaging microscope (Slovak National Museum – The Natural History Museum in Bratislava, Slovakia. Raman spectra of the investigated minerals were excited by a 532 nm frequency-doubled Nd:YVO4 DPSS laser, focused through a $50\times$ objective, and collected in confocal mode using a 25 µm pinhole and an EMCCD detector. Approximately 10 spectra were acquired from the mineral phases investigated at a laser power of 10-20 mW for between 0.5 and 2 s (20 scans for a cycle). The Raman spectra were acquired in the wavenumber range 80-4000 cm⁻¹. The processing of spectra (including fitting by Voigt func-

tions) was carried out using the Thermo Fisher Scientific *OMNIC v. 9.11* software package.

4. Results

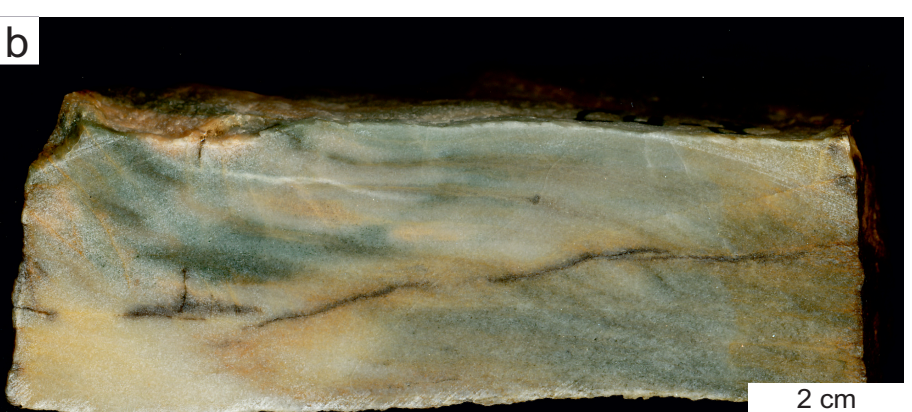
The barium-rich mineralisation at the Čučma – Čierna baňa deposit occurs within metacarbonate lenses associated with graphite- and quartz-muscovite phyllites, metalydites and related manganese mineralisation. The metacarbonates range in colour from white to grey (Fig. 2a) with areas rich in silicates displaying a distinct greenish hue (Fig. 2b, c). Localised orange

to dark brown colouring results from secondary (hydro) oxy minerals. Metacarbonates are mostly composed of calcite (up to 94.2 mol. % CaCO₃), with only minor amounts of other components (MnCO₃ up to 5.6 mol. %; FeCO₃ up to 2.5 mol. %; MgCO₃ up to 2.4 mol. %) (ESM1), quartz occurs only rarely.



4.1. Cymrite

Cymrite in thin sections associated with Ba-rich muscovite and celsian. It forms fine colourless to white elongated prismatic and tabular crystals with vitreous lustre approximately up to 200 µm in length. Cymrite forms subparallel mostly oneway directed aggregates dispersed in metacarbonate matrix associated with Ba-rich muscovite, celsian and clinochlore. It typically exhibits cleavage parallel to (001), along with a less distinct secondary cleavage also oriented along (001) (Fig. 3a, b). In BSE imaging, cymrite shows neither inclusions nor compositional zoning (Fig. 4a, b, c, d). The chemical composition is relatively stable



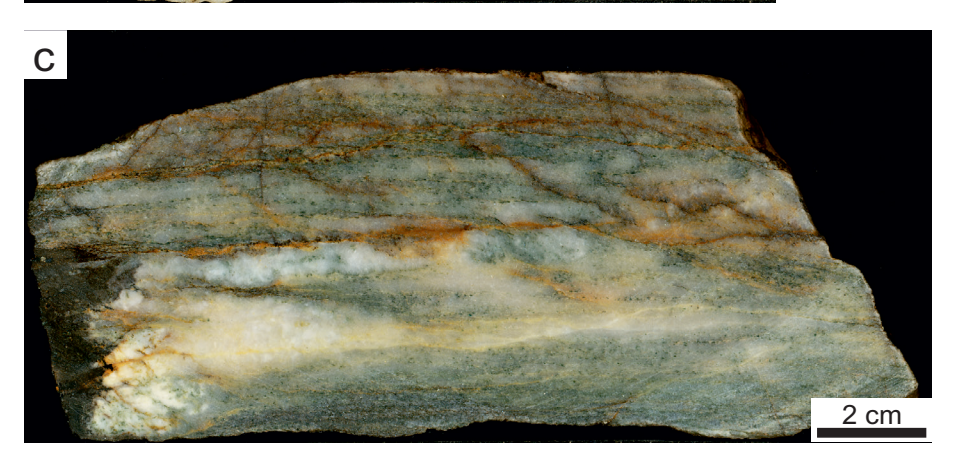


Fig. 2 Representative samples of massive to finely laminated white to light orange marbles (a), the green coloration (b-c) is caused by the accumulation of cymrite, Ba-rich muscovite, celsian, and chlorite.

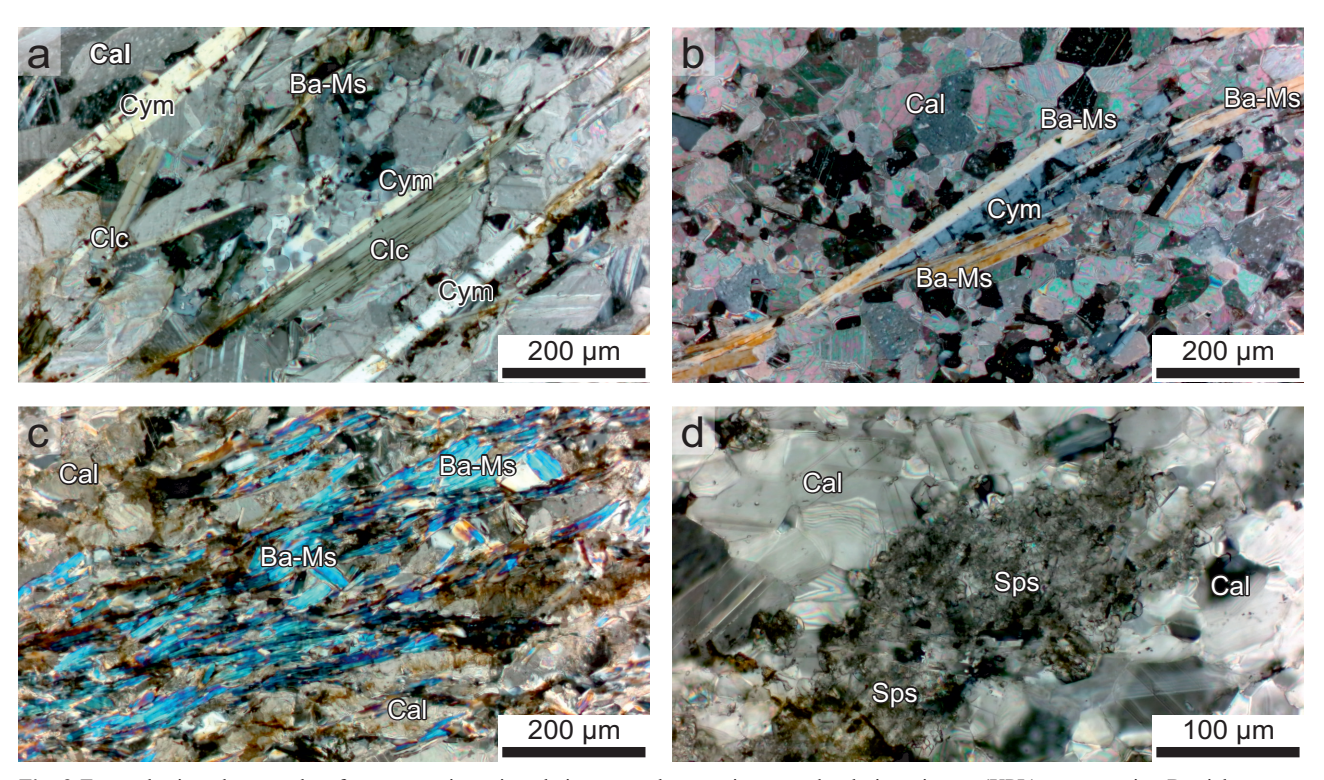


Fig. 3 Textural microphotographs of representative minerals in metacarbonates in crossed polarisers image (XPL): \mathbf{a} – cymrite, Ba-rich muscovite and clinochlore, \mathbf{b} – Cymrite coexisting with Ba-muscovite, \mathbf{c} – Ba-rich muscovite zone, \mathbf{d} – spessartine aggregates. Abbreviations: Ba-rich muscovite (Ba-Ms), calcite (Cal), clinochlore (Clc), cymrite (Cym), spessartine (Sps).

Table 1 Representative and average chemical analyses of cymrite from Čučma (in wt. %) with calculated formulae on the basis of 8 O atoms (*apfu*). Symbol * represents calculation of H,O from (OH).

Analysis	1	2	3	4	5	6	7	8	9	10	Average $(n = 111)$
SiO ₂	33.40	30.00	31.24	32.01	30.87	32.04	31.68	31.39	33.92	30.77	31.67
Al_2O_3	26.14	24.90	25.56	26.55	25.50	26.43	26.22	25.73	24.07	23.86	25.67
FeO	0.04	0.21	0.22	0.04	0.18	0.19	1.26	0.22	0.05	0.05	0.14
MnO	0.00	0.21	0.00	0.12	1.93	0.06	0.13	0.00	0.00	0.00	0.12
MgO	0.00	0.00	0.01	0.00	0.02	0.02	0.70	0.00	0.00	0.00	0.01
CaO	0.02	3.43	1.49	0.20	0.10	0.39	0.35	0.02	0.13	0.19	0.32
SrO	_	-	_	_	_	_	_	0.00	0.19	0.00	0.01
BaO	38.09	36.91	38.10	39.23	38.17	39.65	37.16	40.65	38.76	40.16	38.92
Na ₂ O	0.27	0.11	0.09	0.08	0.06	0.07	0.07	0.09	0.40	0.13	0.09
K_2O	0.68	0.21	0.19	0.21	0.21	0.23	0.16	0.11	0.67	0.28	0.27
H_2O*	2.41	2.30	2.37	2.38	2.32	2.39	2.39	2.33	2.37	2.25	2.34
C1	0.00	0.00	0.02	0.00	0.00	0.00	0.00	-	-	-	0.01
-O=C1	0.00	0.00	0.00	0.00	0.00	0.00	0.00	-	-	-	0.00
Total	101.05	98.28	99,29	100.82	99.36	101.45	100.11	100.55	100.56	97.70	99.55
Si ⁴⁺	2.076	1.954	1.993	2.018	1.993	2.014	1.994	2.016	2.142	2.051	2.029
$^{IV}A1^{3+}$	1.915	1.911	1.922	1.973	1.940	1.958	1.944	1.948	1.792	1.874	1.939
Fe^{2+}	0.002	0.011	0.011	0.002	0.010	0.010	0.067	0.012	0.002	0.003	0.007
Mn^{2+}	0.000	0.012	0.000	0.007	0.106	0.003	0.007	0.000	0.000	0.000	0.007
Mg^{2+}	0.000	0.000	0.001	0.000	0.002	0.002	0.066	0.000	0.000	0.000	0.001
Ca^{2+}	0.001	0.239	0.103	0.013	0.007	0.026	0.024	0.001	0.009	0.014	0.022
Sr^{2+}	_	_	_	_	_	_	_	0.000	0.007	0.000	0.000
Ba^{2+}	0.928	0.943	0.963	0.969	0.966	0.977	0.917	1.023	0.959	1.049	0.978
Na^{+}	0.033	0.013	0.011	0.010	0.008	0.008	0.008	0.011	0.049	0.017	0.011
$K^{\scriptscriptstyle +}$	0.054	0.017	0.017	0.017	0.017	0.018	0.013	0.009	0.054	0.024	0.022
Cl-	0.000	0.000	0.002	0.000	0.000	0.000	0.000	_	_	_	0.001
OH-	1.000	1.000	0.998	1.000	1.000	1.000	1.000	1.000	1.000	1.000	1.000

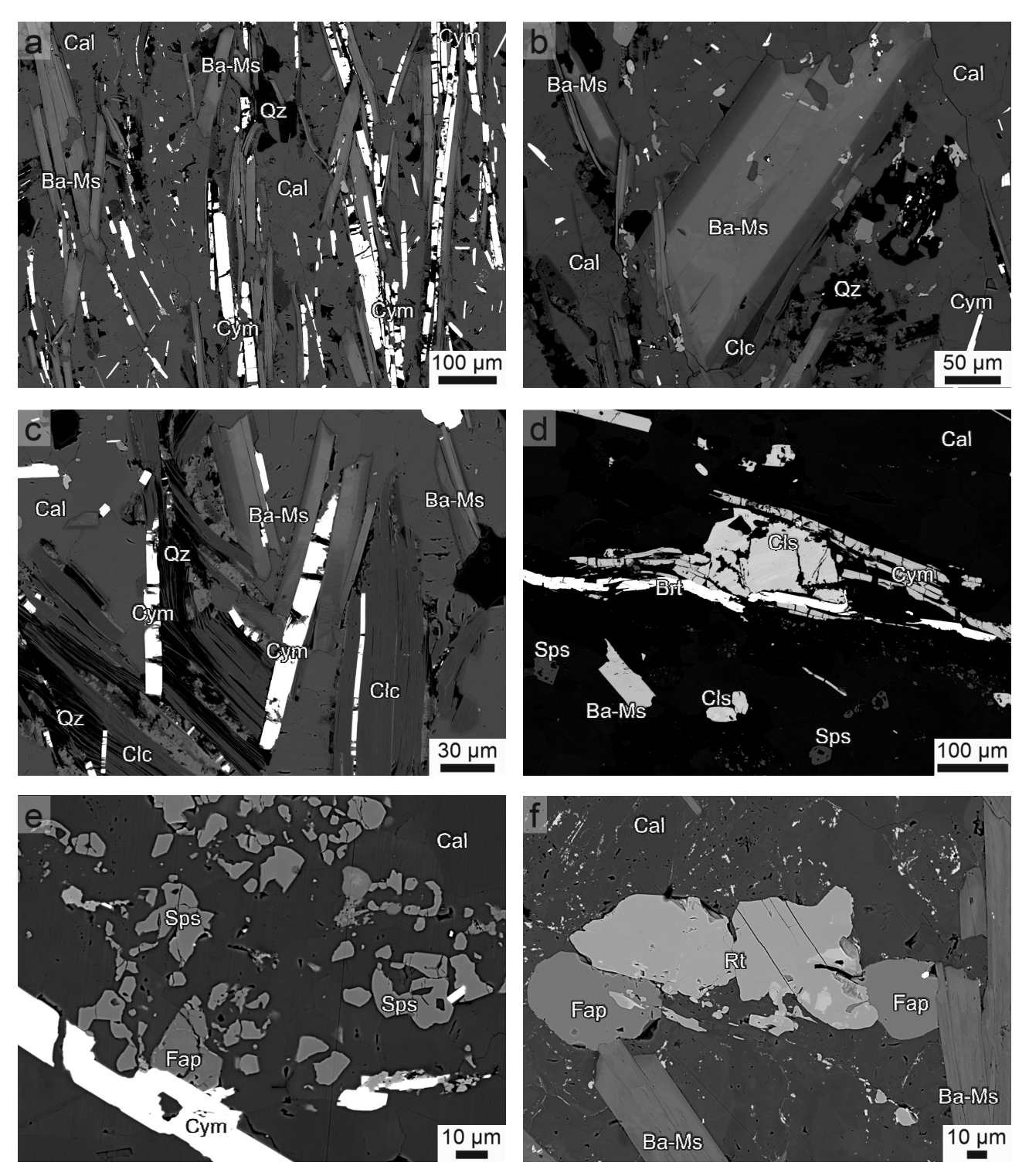


Fig. 4 BSE images of dominant and accessory minerals in metacarbonates: \mathbf{a} – fibrous crystals of cymrite and Ba-rich muscovite, \mathbf{b} – zoned Ba-rich muscovite partially replaced by clinochlore, \mathbf{c} – cymrite, Ba-rich muscovite and clinochlore with quartz, \mathbf{d} – slightly zoned celsian aggregate within cymrite and baryte associated with isolated spessartine, \mathbf{e} – euhedral spessartine crystals with cymrite and fluorapatite, \mathbf{f} – accessory rutile with fluorapatite and Ba-rich muscovite. Abbreviations: Ba-rich muscovite (Ba-Ms), baryte (Brt) calcite (Cal), celsian (Cls), clinochlore (Clc), cymrite (Cym), fluorapatite (Fap), quartz (Qz), rutile (Rt), spessartine (Sps).

with Si (1.95–2.14 apfu), Al (1.79–1.99 apfu) and Ba (0.92–1.05 apfu). The greatest enrichment comes in Ca (up to 0.24 apfu), followed by Mn (up to 0.11 apfu) and

Fe (up to 0.07 apfu). Small enrichment also shows Na and K (both up to 0.05 apfu). Average crystal-chemical formula calculated on the basis of 8 oxygen atoms

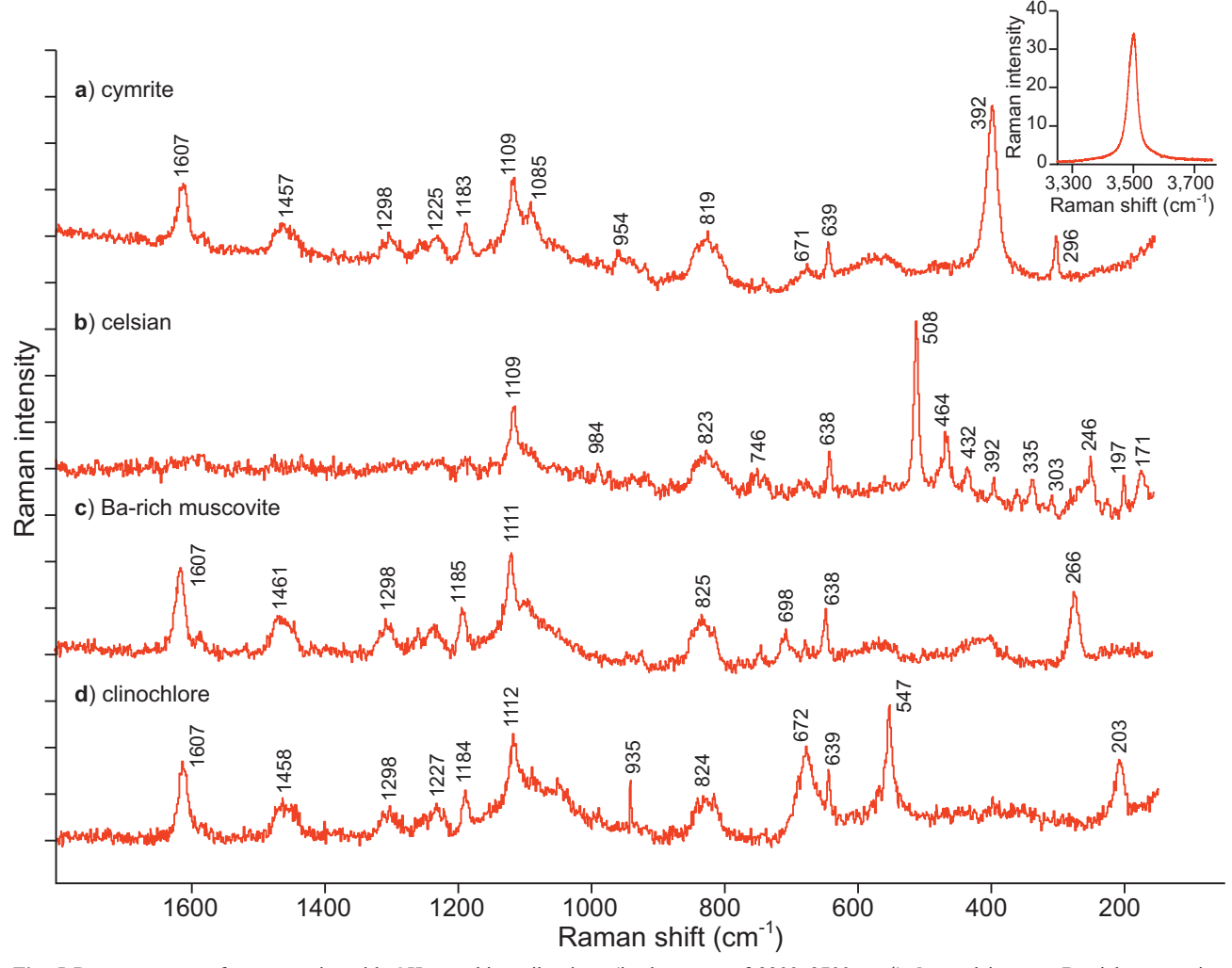


Fig. 5 Raman spectra of: \mathbf{a} – cymrite with OH-stretching vibrations (in the range of 3300–3700 cm⁻¹), \mathbf{b} – celsian, \mathbf{c} – Ba-rich muscovite, \mathbf{d} – clinochlore, in the range of 150–1800 cm⁻¹.

(n=111) is close to the theoretical one and can be expressed as $(Ba_{0.98}Ca_{0.02}K_{0.02}Na_{0.01})(Al_{1.94}Fe_{0.01}Mn_{0.01}Mg_{0.01})$ $Si_{2.02}(O,OH)_8 \cdot H_2O$ (Tab. 1, ESM1). The Raman spectrum is shown in Fig. 5a, bands are identified at 296, 392, 639, 671, 954, 1085, 1109, 1183, 1225, 1298, 1457 and 1607 cm⁻¹. The sharp band near ~3500 cm⁻¹ is assigned to OH stretching vibrations of molecular H₂O.

4.2. Celsian

Celsian forms anhedral grains up to 150 µm in size associated with cymrite, Ba-rich muscovite and baryte. Celsian is present to a lesser content than other silicates, forms solid grains with no lamellae and its colour seems to be more yellowish. Celsian was observed to be enclosed by cymrite along the corroded celsian edges. In BSE imaging, celsian is slightly irregularly zoned (Fig. 4d). The chemical composition is monotonous, where Si (1.98–2.11 apfu), Al (1.83–2.00 apfu) and Ba

(0.90–1.00 apfu) are dominant constituents, with slightly elevated Na (up to 0.06 apfu), K (up to 0.06 apfu), Ca (up to 0.04 apfu) and Sr (up to 0.01 apfu) contents in M-site and Fe³+ (up to 0.02 apfu) at T-site. This chemical composition corresponds to the dominant celsian endmember (89.0–97.3 mol. %) with minimal orthoclase (up to 3.5 mol. %), albite (up to 2.3 mol. %) or anorthite (1.3 mol. %) components. Average crystal-chemical formula based on 8 oxygen atoms (n = 34) can be expressed as ${}^{M}(Ba_{0.96}K_{0.04}Na_{0.02}Ca_{0.01}Sr_{0.01})^{T}(Al_{1.93}Si_{2.05})O_{8}$ (Tab. 2, ESM1). The Raman spectrum is shown in Fig. 5b, bands are identified at 171, 197, 246, 303, 335, 392, 432, 464, 508, 638, 746, 823, 984, 1109, 1183, 1293, 1459 and 1607 cm^{-1} .

4.3. Ba-rich muscovite

Muscovite is widespread mineral in metacarbonate bodies, it forms elongated tabular to fine lamellar crystals

Table 2 Representative and average chemical analyses of celsian from Čučma (in wt. %) with calculated formulae on the basis of 8 O atoms (apfu) and end-members (mol. %).

Analysis	1	2	3	4	5	6	7	8	9	10	Average (n = 34)
P_2O_5	0.00	0.00	0.04	0.00	0.00	0.00	0.00	0.02	0.00	0.00	0.00
SiO_2	33.46	34.42	32.94	32.48	32.48	33.19	32.09	31.77	33.82	33.16	33.06
Al_2O_3	26.69	26.48	26.42	27.13	26.94	26.03	26.99	27.23	24.95	24.88	26.43
Fe_2O_3	0.06	0.07	0.04	0.47	0.14	0.08	0.11	0.00	0.08	0.05	0.08
MnO	0.00	0.07	0.00	0.00	0.00	0.06	0.00	0.00	0.00	0.08	0.01
MgO	0.00	0.00	0.00	0.07	0.00	0.00	0.00	0.00	0.00	0.03	0.01
CaO	0.15	0.16	0.57	0.05	0.10	0.38	0.21	0.20	0.16	0.48	0.21
SrO	0.13	0.25	0.10	0.09	0.18	0.33	0.06	0.00	0.19	0.08	0.13
BaO	39.22	38.02	39.24	40.37	40.01	38.34	40.81	41.00	39.88	40.74	39.49
Na ₂ O	0.21	0.32	0.16	0.11	0.20	0.22	0.05	0.12	0.50	0.18	0.20
K_2O	0.56	0.81	0.41	0.22	0.25	0.67	0.10	0.06	0.56	0.44	0.46
Total	100.48	100.60	99.90	101.00	100.30	99.29	100.42	100.40	100.14	100.12	100.09
P^{5+}	0.000	0.000	0.002	0.000	0.000	0.000	0.000	0.001	0.000	0.000	0.000
Si^{4+}	2.054	2.089	2.040	2.003	2.020	2.062	2.000	1.983	2.103	2.082	2.047
$A1^{3+}$	1.931	1.892	1.928	1.972	1.963	1.904	1.982	2.003	1.830	1.840	1.928
Fe ³⁺	0.003	0.003	0.002	0.022	0.007	0.005	0.005	0.000	0.004	0.003	0.004
Sum T	3.987	3.985	3.972	3.997	3.990	3.971	3.987	3.988	3.937	3.924	3.979
$Mn^{2^{+}}$	0.000	0.004	0.000	0.000	0.000	0.003	0.000	0.000	0.000	0.004	0.001
Mg^{2+}	0.000	0.000	0.000	0.007	0.000	0.000	0.000	0.000	0.000	0.003	0.001
Ca^{2+}	0.010	0.011	0.038	0.003	0.007	0.025	0.014	0.013	0.011	0.032	0.014
Sr^{2+}	0.004	0.009	0.004	0.003	0.006	0.012	0.002	0.000	0.007	0.003	0.005
Ba^{2+}	0.943	0.903	0.952	0.976	0.965	0.931	0.997	1.003	0.971	1.002	0.958
Na^+	0.025	0.038	0.019	0.013	0.023	0.027	0.006	0.014	0.060	0.022	0.024
K^+	0.044	0.063	0.033	0.017	0.020	0.053	0.008	0.005	0.045	0.035	0.037
Sum M	1.027	1.027	1.045	1.019	1.021	1.051	1.027	1.036	1.093	1.101	1.038
Cls	92.30	89.03	91.42	96.70	95.11	89.87	97.29	96.84	89.39	91.82	92.85
Or	4.31	6.18	3.13	1.72	1.93	5.13	0.80	0.48	4.12	3.20	3.54
Ab	2.40	3.74	1.81	1.26	2.29	2.60	0.55	1.37	5.50	2.03	2.29
An	0.98	1.05	3.64	0.32	0.66	2.40	1.36	1.30	1.00	2.94	1.32

of white to strongly silvery white colour with vitreous lustre. Muscovite is closely associated with cymrite, celsian and clinochlore, while it mostly forms one-way directed aggregates oriented parallel to the metacarbonate layering (Fig. 3a-c). As it is nearly always overgrown with clinochlore, zones rich-in muscovite can be macroscopically distinguished by its light green colour. In BSE images muscovite shows strong chemical zoning. In smaller crystal aggregates muscovite is generally light (Fig. 4a), the bigger aggregates can be generally attributed to two zones (Fig. 4b, c). BSE dark zones are mostly formed along the crystal edges, while light zones are predominantly forming inner parts of crystals. In the BSE dark zone lower contents of Ba (up to 0.14-0.21 apfu) compensated mostly by increased K (up to 0.77 apfu) can be observed compared to BSE light zone (0.25–0.32 apfu Ba) and decreased K (up to 0.65 apfu). Contents of Fe and Mg are relatively similar (up to 0.21 Mg apfu and up to 0.09 Fe apfu in BSE dark zone; up to 0.19 Mg apfu and 0.12 Fe apfu in BSE light zone) (Tab. 3, ESM1). The Raman spectrum of Ba-rich muscovite (BSE light zone) is shown in Fig. 5c, bands are identified at 266, 638, 398, 825, 1111, 1185, 1298, 1461 and 1607 cm⁻¹.

4.4. Clinochlore

Clinochlore is common in metacarbonates, where it forms fine acicular crystals up to 100 µm in size (Fig. 4c) grouped to the bigger aggregates. Clinochlore is in thin sections distinguishable by its light green colour (Fig. 3a) causing macroscopically green colour of enriched zones in marbles. Clinochlore is homogeneous in BSE (Fig. 4c), its chemical composition investigated by 25 chemical analyses shows dominant Mg (2.31–3.17 *apfu*) over minor Fe (1.59–2.15 *apfu*), with very small amount of Mn (up to 0.10 *apfu*) in *A*-site and content of Ba below 0.01 *apfu* (Tab. 4, ESM1). The Raman spectrum is shown in Fig. 5d, bands are identified at 203, 547, 639, 672, 824, 935, 1112, 1184, 1227, 1298, 1458 and 1607 cm⁻¹.

4.5. Baryte

Baryte represents relatively scarce phase, it was identified in the form of isolated aggregates up to $10~\mu m$, more extensively it was observed in thin veinlets (Fig. 4d). Baryte is non-zoned and its chemical composition is close to ideal end-member formula with only minor

Table 3 Representative and average chemical analyses of Ba-rich muscovite from Čučma (in wt. %) with calculated on the basis of 11 O atoms (apfu). Symbol * represents calculation of H₂O from (OH)⁻, mgli calculated as (Mg-Li), feal calculated as (V¹Fe_{tot}+Mn+Ti)-V¹Al.

TiO_2^2 0.13	44.39 0.46	dark zone 43.14			Average $(n = 23)$			11. 1 /			Average $(n = 49)$
TiO ₂ 0.13 Al ₂ O ₃ 31.62 Cr ₂ O ₃ 0.00 FeO 1.77 MnO 0.03 MgO 2.01 CaO 0.08 BaO 6.60 Na ₂ O 0.27 K ₂ O 6.98 H ₂ O* 4.29 Cl 0.01		43.14	4400					light zon	e		8 (1)
$\begin{array}{cccc} Al_2O_3 & 31.62 \\ Cr_2O_3 & 0.00 \\ FeO & 1.77 \\ MnO & 0.03 \\ MgO & 2.01 \\ CaO & 0.08 \\ BaO & 6.60 \\ Na_2O & 0.27 \\ K_2O & 6.98 \\ H_2O^* & 4.29 \\ Cl & 0.01 \\ \end{array}$	0.46		44.90	45.15	44.54	41.57	40.57	41.32	40.11	42.99	40.87
$\begin{array}{ccc} \text{Cr}_2\text{O}_3 & 0.00 \\ \text{FeO} & 1.77 \\ \text{MnO} & 0.03 \\ \text{MgO} & 2.01 \\ \text{CaO} & 0.08 \\ \text{BaO} & 6.60 \\ \text{Na}_2\text{O} & 0.27 \\ \text{K}_2\text{O} & 6.98 \\ \text{H}_2\text{O}^* & 4.29 \\ \text{Cl} & 0.01 \\ \end{array}$		0.50	0.22	0.20	0.20	0.29	0.62	0.69	0.75	0.51	0.54
$\begin{array}{ccc} \text{Cr}_2\text{O}_3 & 0.00 \\ \text{FeO} & 1.77 \\ \text{MnO} & 0.03 \\ \text{MgO} & 2.01 \\ \text{CaO} & 0.08 \\ \text{BaO} & 6.60 \\ \text{Na}_2\text{O} & 0.27 \\ \text{K}_2\text{O} & 6.98 \\ \text{H}_2\text{O}^* & 4.29 \\ \text{Cl} & 0.01 \\ \end{array}$	30.52	31.88	31.64	31.32	31.63	32.74	32.46	33.17	32.33	31.81	32.80
FeO 1.77 MnO 0.03 MgO 2.01 CaO 0.08 BaO 6.60 Na ₂ O 0.27 K ₂ O 6.98 H ₂ O* 4.29 Cl 0.01	0.00	0.00	0.04	0.00	0.01	0.00	0.08	0.00	0.00	0.00	0.02
MgO 2.01 CaO 0.08 BaO 6.60 Na ₂ O 0.27 K ₂ O 6.98 H ₂ O* 4.29 Cl 0.01	2.52	1.58	1.37	1.64	1.59	1.57	1.86	1.70	1.81	1.89	1.73
$\begin{array}{ccc} CaO & 0.08 \\ BaO & 6.60 \\ Na_2O & 0.27 \\ K_2O & 6.98 \\ H_2O^* & 4.29 \\ Cl & 0.01 \\ \end{array}$	0.08	0.05	0.00	0.07	0.06	0.12	0.03	0.04	0.00	0.03	0.06
$\begin{array}{ccc} BaO & 6.60 \\ Na_2O & 0.27 \\ K_2O & 6.98 \\ H_2O^* & 4.29 \\ Cl & 0.01 \\ \end{array}$	2.14	1.87	2.12	2.16	2.06	1.57	1.67	1.32	1.38	1.83	1.53
$\begin{array}{lll} \text{Na}_2\text{O} & 0.27 \\ \text{K}_2\text{O} & 6.98 \\ \text{H}_2\text{O}^* & 4.29 \\ \text{Cl} & 0.01 \end{array}$	0.09	0.06	0.04	0.35	0.17	0.12	0.08	0.03	0.07	0.25	0.09
K_2O 6.98 H_2O^* 4.29 Cl 0.01	7.13	7.70	5.91	5.20	6.17	9.05	10.27	10.56	11.13	9.70	10.00
H ₂ O* 4.29 Cl 0.01	0.43	0.28	0.21	0.27	0.31	0.45	0.50	0.57	0.52	0.37	0.55
Cl 0.01	7.20	7.77	8.42	8.51	8.21	7.13	6.49	6.18	5.71	5.09	6.44
	4.27	4.25	4.32	4.33	4.30	4.19	4.15	4.21	4.10	4.22	4.17
-0=C1 0.00	0.00	0.01	0.01	0.00	0.00	0.00	0.00	0.00	0.01	0.01	0.00
0 01 0100	0.00	0.00	0.00	0.00	0.00	0.00	0.00	0.00	0.00	0.00	0.00
Total 98.51	99.23	99.07	99.18	99.18	99.26	98.80	98.78	99.80	97.91	98.70	98.79
Si ⁴⁺ 3.124	3.116	3.045	3.119	3.129	3.103	2.972	2.929	2.944	2.929	3.051	2.938
$A1^{3+}$ 0.876	0.884	0.955	0.881	0.871	0.897	1.028	1.071	1.056	1.071	0.949	1.062
Sum <i>T</i> 4.000	4.000	4.000	4.000	4.000	4.000	4.000	4.000	4.000	4.000	4.000	4.000
Ti ⁴⁺ 0.007	0.024	0.026	0.011	0.010	0.011	0.016	0.034	0.037	0.041	0.027	0.029
Al ³⁺ 1.728	1.641	1.697	1.709	1.688	1.700	1.730	1.691	1.729	1.711	1.712	1.718
Cr^{3+} 0.000	0.000	0.000	0.002	0.000	0.000	0.000	0.004	0.000	0.000	0.000	0.001
Fe^{2+} 0.103	0.148	0.093	0.080	0.095	0.093	0.094	0.112	0.101	0.110	0.112	0.104
Mn^{2+} 0.002	0.005	0.003	0.000	0.004	0.004	0.007	0.002	0.002	0.000	0.002	0.004
Mg^{2+} 0.209	0.224	0.197	0.220	0.223	0.214	0.167	0.180	0.140	0.150	0.193	0.164
Sum <i>M</i> 2.050	2.043	2.016	2.023	2.020	2.021	2.014	2.024	2.009	2.013	2.046	2.020
Ba ²⁺ 0.181	0.196	0.213	0.161	0.141	0.169	0.254	0.290	0.295	0.318	0.270	0.282
Ca^{2+} 0.006	0.007	0.004	0.003	0.026	0.012	0.009	0.006	0.003	0.005	0.019	0.007
Na ⁺ 0.037	0.058	0.038	0.028	0.036	0.042	0.063	0.070	0.079	0.074	0.050	0.076
K ⁺ 0.622	0.645	0.699	0.746	0.752	0.730	0.650	0.598	0.562	0.532	0.461	0.591
□ 0.154	0.094	0.045	0.062	0.045	0.047	0.024	0.036	0.062	0.071	0.200	0.045
Sum <i>I</i> 0.846	0.906	0.955	0.938	0.955	0.953	0.976	0.964	0.938	0.929	0.800	0.955
Cl- 0.001	0.000	0.001	0.001	0.000	0.000	0.000	0.000	0.000	0.001	0.001	0.000
OH- 1.999	2.000	1.999	1.999	2.000	2.000	2.000	2.000	2.000	1.999	1.999	2.000
Sum <i>A</i> 2.000	2.000	2.000	2.000	2.000	2.000	2.000	2.000	2.000	2.000	2.000	2.000
mgli 0.209	0.00:	0.197	0.220	0.223	0.214	0.167	0.180	0.140	0.150	0.193	0.164
feal -1.616	0.224 -1.464	0.197	0.220	0.223	0.21.	-1.614					-1.581

elevation in Sr, Ca and Fe (all up to 0.01 apfu) (Tab. 5, ESM1).

4.6. Spessartine

Spessartine was observed rarely, it forms not very well developed anhedral crystals up to 30 μ m in size (Fig. 4e), grouped to the bigger accumulations up to 300 μ m in size (Fig. 4d). In thin sections they are transparent with strong relief, macroscopically they show very soft light yellow colour. Spessartine does not show a regular occurrence with any silicate phases; it occurs rather randomly in metacarbonates. In BSE spessartine crystals are nonzoned and their chemical composition is variable with dominant spessartine molecule (up to 60.0 mol. %), and

it shows significantly increased grossular (up to 31.6 mol. %) and almandine (up to 18.0 mol. %), whereas other components are under 3.0 mol. % (ESM1).

4.7. Accessory phases (fluorapatite, rutile)

Fluorapatite occurs rarely as it forms subhedral non-zoned grains up to 50 μ m in size (Fig. 4f). Chemical composition in monotonous close to ideal end-member formula with Σ REE not exceeding 0.01 apfu (ESM1). Rutile reaches size up to 100 μ m and on the other hand is dominantly non-zoned, but locally it contains areas enriched with Fe (up to 0.02 apfu), Nb (up to 0.01 apfu) and W (up to 0.01 apfu) (ESM1), causing a slight chemical zoning in BSE (Fig. 4f).

Table 4 Representative and average chemical analyses of clinochlore from Čučma (in wt. %) with calculated formulae on the basis of 14 O atoms (*apfu*). Symbol * represents calculation of H₂O from (OH).

Analysis	1	2	3	4	5	6	7	8	9	10	Average $(n = 25)$
SiO ₂	25.90	28.03	28.08	27.61	27.31	26.10	25.62	25.83	26.57	28.11	26.78
TiO,	0.05	0.00	0.00	0.00	0.00	0.21	0.18	0.00	0.04	0.02	0.04
Al ₂ O ₃	21.67	22.28	20.20	20.69	22.57	20.82	21.82	21.96	18.92	19.19	20.78
Cr ₂ O ₃	0.05	0.05	0.04	0.14	0.08	0.10	0.00	0.06	0.00	0.00	0.04
FeO	24.12	23.43	22.38	23.45	23.30	23.63	25.02	25.12	18.04	19.95	22.63
MnO	0.54	0.61	0.42	0.75	0.58	0.47	0.67	0.49	1.13	0.44	0.65
MgO	16.90	15.38	17.89	16.77	15.80	17.57	17.14	16.81	20.22	19.23	17.57
CaO	0.47	0.20	0.16	0.14	0.21	0.08	0.11	0.09	0.08	0.12	0.14
BaO	0.00	0.00	0.00	0.02	0.05	0.02	0.01	0.00	0.07	0.11	0.03
Na,O	0.00	0.00	0.00	0.02	0.04	0.00	0.05	0.00	0.02	0.01	0.01
K,O	0.02	0.02	0.02	0.02	0.03	0.00	0.00	0.01	0.00	0.00	0.01
H,O*	11.70	11.89	11.81	11.77	11.81	11.64	11.76	11.74	11.39	11.66	11.67
F	0.00	0.00	0.00	0.00	0.11	0.00	0.00	0.00	_	_	0.01
Cl	0.01	0.01	0.01	0.01	0.01	0.01	0.02	0.02	0.02	0.00	0.01
O=F,Cl	0.01	0.01	0.01	0.01	0.11	0.01	0.02	0.02	0.02	0.00	0.01
Total	101.40	101.87	101.00	101.39	101.78	100.64	102.37	102.11	96.49	98.62	100.33
Si ⁴⁺	2.655	2.828	2.852	2.813	2.762	2.689	2.612	2.637	2.797	2.892	2.752
$^{IV}\!Al^{3+}$	1.345	1.172	1.148	1.187	1.238	1.311	1.388	1.363	1.203	1.108	1.248
Sum T	4.000	4.000	4.000	4.000	4.000	4.000	4.000	4.000	4.000	4.000	4.000
Ti ⁴⁺	0.004	0.000	0.000	0.000	0.000	0.016	0.014	0.000	0.003	0.002	0.003
$^{VI}Al^{3+}$	1.273	1.477	1.270	1.298	1.451	1.217	1.235	1.279	1.145	1.219	1.268
Cr	0.004	0.004	0.003	0.012	0.006	0.008	0.000	0.005	0.000	0.000	0.003
Fe	2.068	1.977	1.901	1.998	1.970	2.036	2.134	2.145	1.589	1.717	1.944
Mn	0.047	0.052	0.036	0.065	0.050	0.041	0.058	0.042	0.100	0.039	0.057
Mg	2.582	2.313	2.708	2.548	2.382	2.699	2.605	2.558	3.174	2.949	2.693
Ca	0.052	0.021	0.018	0.015	0.023	0.009	0.012	0.010	0.009	0.014	0.015
Ba	0.000	0.000	0.000	0.001	0.002	0.001	0.000	0.000	0.003	0.004	0.001
Na	0.000	0.000	0.000	0.004	0.007	0.000	0.011	0.000	0.004	0.000	0.002
K	0.003	0.002	0.003	0.003	0.004	0.000	0.000	0.000	0.000	0.000	0.001
Sum A	6.032	5.847	5.939	5.942	5.896	6.027	6.068	6.039	6.028	5.943	5.987
F-	0.000	0.000	0.000	0.000	0.034	0.000	0.000	0.000	_	_	0.004
Cl-	0.001	0.001	0.001	0.001	0.001	0.001	0.003	0.003	0.003	0.000	0.001
OH-	7.999	7.999	7.999	7.999	7.965	7.999	7.997	7.997	7.997	8.000	7.996
Sum	8.000	8.000	8.000	8.000	8.000	8.000	8.000	8.000	8.000	8.000	8.000
#Mg	0.56	0.54	0.59	0.56	0.55	0.57	0.55	0.54	0.67	0.63	0.58

5. Discussion

The studied mineral association represented by cymrite, celsian, Ba-rich muscovite, clinochlore, baryte, spessartine, quartz and accessory fluorapatite and rutile serves as unique indicator of diagenetic processes in the precursor sedimentary environment followed by metamorphic development as recorded by textural relations, chemical zoning and phase overgrowths documenting multiple stages of mineral evolution.

5.1. Source of barium in Čučma manganese deposit

The influence of local submarine volcanic activity of basic composition likely accompanied the formation of manganese-enriched sediments along with carbonates and siliceous rocks (lydites) in the Čučma area (Bajaník et al. 1983). Such volcanism with hydrothermal exhalative processes may have generated hydrothermal fluids enriched in Ba. The source of barium should be regarded as a component formed during the early developmental stages of the region, through a combination of sedimentation and volcanism with associated hydrothermal processes (Grecula et al. 1995). This barium was later mobilised by metamorphic processes and incorporated into newly formed metamorphic minerals through recrystallisation. The highest concentrations of Ba are in baryte, Bafeldspar (celsian) and cymrite, while a lesser amount is incorporated into Ba-muscovite, while clinochlore does not contain any Ba (Tab. 1–5, ESM1).

The source of barium in the sheet silicates is generally considered to originate from baryte or Ba-Si-Al gels (McSwiggen et al. 1994). Baryte can be dissolved under

Analysis	1	2	3	4	5	6	7	8	9	10	Average (n = 10)
SO ₃	36.21	34.58	34.34	34.15	34.06	33.88	34.48	32.93	34.75	33.19	34.26
SiO ₂	0.00	0.04	0.00	0.05	0.04	0.20	0.27	0.17	0.00	0.10	0.09
FeO	0.18	0.22	0.34	0.25	0.21	0.45	0.48	0.44	0.11	0.24	0.29
MgO	0.01	0.04	0.02	0.00	0.01	0.04	0.03	0.04	0.03	0.06	0.03
CaO	0.17	0.26	0.20	0.29	0.26	0.35	0.53	0.17	0.32	0.84	0.34
SrO	0.75	0.38	0.53	0.93	1.01	0.44	0.47	0.29	0.76	0.48	0.61
BaO	63.14	64.62	64.27	63.21	63.42	64.03	63.86	65.03	63.98	64.02	63.96
Total	100.56	100.24	99.77	98.91	99.08	99.59	100.28	99.03	100.04	99.59	99.71
S ⁶⁺	1.014	0.997	0.997	0.996	0.994	0.988	0.990	0.981	0.981	0.999	0.991
Si^{4+}	0.000	0.002	0.000	0.002	0.001	0.008	0.010	0.005	0.004	0.000	0.003
Sum	1.014	0.999	0.997	0.998	0.996	0.996	1.000	0.987	0.985	0.999	1.002
Ba ²⁺	0.931	0.972	0.973	0.962	0.965	0.972	0.954	1.010	0.959	0.977	0.967
Sr^{2+}	0.016	0.008	0.012	0.021	0.023	0.010	0.010	0.007	0.017	0.011	0.014
Ca^{2+}	0.007	0.011	0.008	0.012	0.011	0.015	0.022	0.007	0.013	0.035	0.014
Fe^{2+}	0.006	0.007	0.011	0.008	0.007	0.015	0.015	0.015	0.003	0.008	0.009
Mg^{2+}	0.001	0.002	0.001	0.000	0.001	0.002	0.002	0.002	0.002	0.004	0.002
Sum	0.951	1.000	1.005	1.003	1.006	1.013	1.004	1.041	0.994	1.034	1.005

Table 5 Representative and average chemical analyses of baryte from Čučma (in wt. %) with calculated formulae on the basis of 4 O atoms (apfu).

reducing conditions during diagenetic and metamorphic events and the released barium may precipitate in the form of Ba-rich sheet silicates, as noted by Tracy (1991). However, baryte may remain stable under reducing conditions in a calcium-rich environment. The coexistence of baryte and hydrous Ba-silicates has been confirmed in unmetamorphosed sediments of northern Greenland (Jakobsen 1990), where these minerals formed during diagenesis under reducing conditions, as evidenced by the presence of pyrite and organic matter.

5.2. Origin and phase relations of Ba-rich mineralisation

The first stage represents the deposition of sediments, primarily pelitic (i.e., clay-rich) with a contribution of an organic components (black shales including carbonates and siliceous material) influenced by hydrothermal activity associated with concurrent submarine basic volcanic processes. The character of sedimentation, including diagenetic processes, was defined by a cyclic alteration of individual sedimentary layers, namely interbedding of clayey-organic pelites with carbonates and siliceous rocks, within flysch-like zones. These sequences were occasionally disrupted by basic pyroclastic material depositions, leading to the formation of volcano-sedimentary horizons of variable thickness (Bajaník et al. 1983).

The second stage was initiated by Variscan regional metamorphism, which caused the recrystallisation of the compact flysch-like sequences. These retained their original flysch textures, although their mineral composition was strongly changed. Recrystallisation also triggered barium mobility probably from precursor baryte. During metamorphism, both prograde and retrograde stages occurred, representing the Variscan and Alpine

orogenic cycles (Bajaník et al. 1983; Vozárová 1993). Original detrital feldspars may have been present during primary sedimentation, forming part of the clastic clay-rich sediments. Ba feldspars crystallised during the prograde stage of Variscan metamorphism. The distribution of Ba between feldspars and micas differentiated due to distribution coefficients at given pTx conditions. The majority entered feldspar structures, likely due to their structural preference, while a smaller proportion of the total Ba entered newly-forming micas.

Micas originally formed via recrystallisation of K-rich clay minerals, which became enriched in barium during this process. Only muscovite was present, no phlogopite or other micas were identified, indicating that recrystallisation occurred under low-temperature conditions, allowing Ba to be incorporated solely into newly forming muscovite. Ba-rich muscovite, as well as cymrite, is commonly found in manganese-enriched metamorphic rocks. It forms during the recrystallisation of sediments containing manganese and barium, often in association with hydrothermal activity, as documented by Das Gupta et al. (1970). The presence of Ba-muscovite in marbles has also been confirmed in Franklin Marble, Lime Crest and Sterling Hill in New Jersey (Tracy 1991).

Cymrite and celsian are known to be products of interaction of Ba (and K) with water depending on the partial water and hydrostatic pressure (Seki, Kennedy 1964). Available experimental data on the reversible dehydration equilibrium between BaAl₂Si₂O₈·H₂O (cymrite) and BaAl₂Si₂O₈ (celsian) + H₂O (Essene 1967; Nitsch 1980; Graham et al. 1992) are variable in different metamorphic environments. The stability and growth kinetics of celsian and cymrite are described within the BaO–Al₂O₃–SiO₂–H₂O system (Graham et al. 1992) with high barium activity (Sorokhtina et al. 2008). Nitsch (1980) established

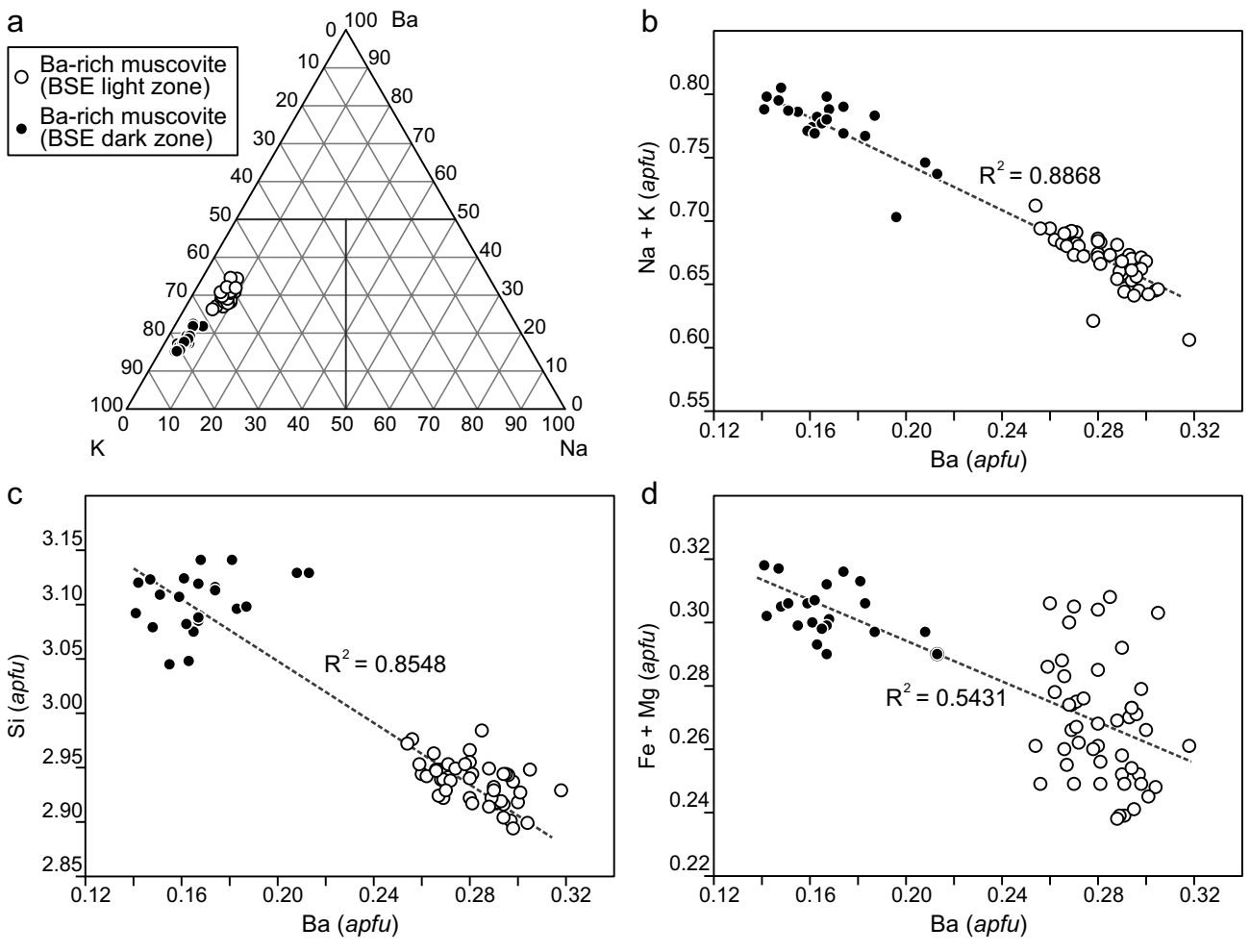


Fig. 6 Composition variation diagrams for Ba-rich muscovite: \mathbf{a} – Ternary plot of the interlayer cations from Ba-rich muscovite, \mathbf{b} – Na+K vs. Ba (apfu), \mathbf{c} – Fe+Mn vs. Ba (apfu), \mathbf{d} – Si vs. Ba (apfu), with correlation coefficients \mathbb{R}^2 .

equilibrium between cymrite and celsian at 400 MPa and 360 °C, and at 700 MPa and 525 °C. Cymrite is generally regarded as the hydrated equivalent of celsian and is associated with barium-rich rocks that have undergone low-grade metamorphism. An example is the stability of cymrite in the Paleozoic baryte deposit in Zamora, Spain, at 350-370 °C and 150 MPa (Moro et al. 2001), where stability field of cymrite was confirmed to be stable in low p-T metasedimentary environments. Furthermore, Hsu (1994) demonstrated that baryte can be entirely replaced by cymrite under pressure-temperature conditions below 315 °C and 300 MPa, in the presence of an alkaline hydrothermal solution rich in dissolved Si and Al circulating through carbonate rocks. This transformation occurs via the reaction $BaSO_4 + Al_2O_3 + 2SiO_2 + 2OH^- =$ BaAl₂Si₂O₈·H₂O+SO₄²-. In this process, sulfate ions may act as precursors for sulfides, suggesting an alternative pathway for cymrite formation during the early stages of metamorphic mineralisation. However, based on textural evidence at the studied associating rocks of Čučma manganese deposit, cymrite plates were preferentially observed around corroded celsian grain boundaries (Fig. 4d), therefore it is more likely that the majority of the present cymrite formed via hydration reaction at the expense of celsian.

5.3. Chemical and structural characteristics of Ba-rich minerals

The chemical composition of celsian and cymrite are close to the end-member formulae, with only small amount of K (up to 0.05 *apfu*) in cymrite further demonstrates the absence of the synthesised high-pressure hexagonal analogue – *K-cymrite* (Šontevska et al. 2007; Romanenko et al. 2024). Muscovite, ideally (KAl₂(AlSi₃O₁₀) (OH)₂) exhibit solid-solution toward its intermediate Ba-analogue ganterite ideally (Ba_{0.5}K_{0.5})Al₂(Al_{1.5}Si_{2.5}) O₁₀(OH)₂. Chemical analyses of Ba-rich muscovite from Čučma show interlayer *I*-site Ba content up to 0.32 *apfu* (Tab. 3, ESM1) with no elevated tetrahedral Al and therefore are considered to be Ba-rich muscovite (Fig. 6a). They reveal several well-known crystal-chemical substi-

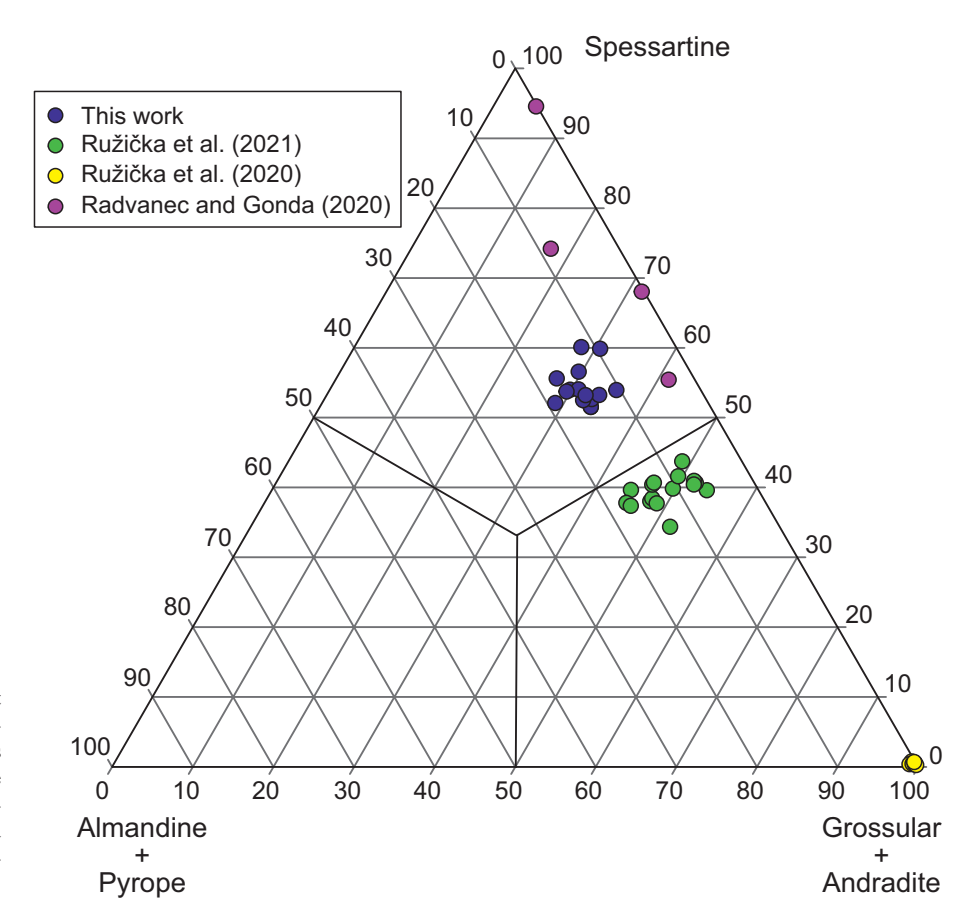


Fig. 7 Classification diagram of garnet group minerals from the Čučma – Čierna baňa manganese deposit. Garnets have been investigated in manganese ore (Radvanec and Gonda 2020), metacarbonate rocks (this study; Ružička et al. 2020), and basalt-derived metapyroclastics (Ružička et al. 2021).

tutions. Barium can be incorporated into the muscovite lattice through multiple independent and coupled substitution mechanisms (Tracy 1991; Grapes 1993; Hetherington et al. 2003; Raith et al. 2014; Moles 2025), while the following substitutions has been considered:

- (1) $Ba^{2+} + {}^{IV}Al^{3+} = (K,Na)^{+} + Si^{4+}$
- (2) $Ba^{2+} + (Fe,Mg)^{2+} = (K,Na)^{+} + Al^{3+}$
- (3) $Ba^{2+} = K^+ + \square$
- (4) $^{VI}(Fe,Mg)^{2+} + Si^{4+} = ^{VI}(Al^{3+},Ti^{4+},Cr^{3+}) + ^{IV}Al^{3+}$

Substitution (1) shown in diagram in Fig. 6b shows very good correlation (with correlation coefficient R² approximately 0.9 for both BSE light and dark zones) and represents probably the most important substitution influencing incorporation of interlayer Ba to muscovite. The structural misfit and interlayer site distortion caused by the coupled substitution (1) is partially compensated by expansion of the octahedral sheet and contraction of the tetrahedral sheet. This adjustment occurs through the concurrent (4) substitution involving the celadonite component (Armbruster et al. 2002). The (1) substitution also demonstrates the participation of ganterite molecule (Fig. 6c). Substitution (2) shown in Fig. 6d, is less apparent with correlation coefficient R² at approximately 0.54 and its presence shows increase in Ba is not always

followed by decrease in Fe and Mg, therefore is not as significant as (1). The substitution (3) is occurring in the interlayer sites and might explain cation deficiency (up to 0.20 apfu) in theoretical 1.00 apfu interlayer A-site occupancy. Clinochlore lacks any content of Ba or K (both below 0.01 apfu; Tab. 4, ESM1), indicating its formation during the final, overprinting retrograde Alpine metamorphic phase. The absence of K in chlorite further indicates the complete replacement of muscovite with no tiny relicts still present or completely newly formed clinochlore.

Spessartine chemical composition (Fig. 7) from studied metacarbonate bodies is spatially closely related to spessartines (up to 95 mol. %) identified from manganese ore (Radvanec and Gonda 2020). Increased grossular (up to 31.6 mol. %) in studied spessartine shows its affinity also to associating basic metavolcanoclastic material identified by Ružička et al. (2021) and with grossular from metacarbonate bodies identified by Ružička et al. (2020). Spessartine crystals likely formed during the early, low-pressure stages of Variscan prograde metamorphism at temperatures ~300 °C (Theye et al. 1996), in close genetic association with manganese ore mineralisation. Subsequent partial resorption of spessartine occurred during retrograde Alpine metamorphic overprinting.

5.4. Raman spectroscopy of Ba-rich minerals

The cymrite bands (Fig. 5a) at the 1607 cm⁻¹ can be assigned to the H-O-H bending region, peak at approximately 3500 cm⁻¹ shows sharp O-H stretching, stretching Si-O-Si vibrations occur in the 1200-900 cm⁻¹ region, 819 cm⁻¹ might be attributed to tetrahedral Al-O stretching, 639 cm⁻¹ might be associated with Ba-OH librations, relatively broader band at the 392 cm⁻¹ probably suggests structural disorder for low to mediate p-T environments and 296 cm⁻¹ can be assigned to Ba-O vibrations (Graham et al. 1992; Šontevska et al. 2007; Romanenko et al. 2024). Similarly, the Raman spectra of celsian (Fig. 5b) are very well known in the range 100-1200 cm⁻¹ to be characteristic bands for feldspars (Freeman et al. 2008). The most prominent band located near 508 cm⁻¹ along with other band in the range of 464 cm⁻¹ are associated with the ring-breathing vibrations of four-membered tetrahedral rings. Additionally, bands around 823 and 1109 cm⁻¹ are attributed to the deformation and stretching vibrations of the tetrahedral units.

6. Conclusions

The Čučma – Čierna baňa manganese deposit hosts within associating metacarbonate lenses an interesting mineral assemblage composed of dominantly (except calcite) Ba-rich phases documenting a polygenic geological processes of sedimentation, volcanism, diagenesis and metamorphism. The metacarbonates are composed of calcite (containing up to 94.2 mol. % CaCO₃) locally enriched in silicates-rich zones. The most significant minerals in these silicates bands include cymrite, celsian, Ba-rich muscovite and baryte, which serve as important indicator of Ba redistribution during metamorphic overprint of the sediments with silicate layers.

Cymrite and celsian show nearly ideal end-member formula chemical compositions and very close textural relationships, where cymrite overgrows or replaces celsian, indicating a formation via hydration reactions during the metamorphism. Ba-rich muscovite forms zoned aggregates oriented with the host foliation of the rock, incorporating additional Ba through multiple discussed substitutions. On the other hand, clinochlore lacks any barium or potassium in structure and represents a complete replacement product of muscovite or newly generated phase during the late-stage metamorphic event. Baryte is considered to be primary source of metamorphic Ba fluids, which was transformed and recrystallised during later-stages of Variscan and Alpine metamorphism. The presence of spessartine indicates a close relation with associated manganese mineralisation as well as accessory fluorapatite and rutile illustrates the complexity of the entire mineralisation. Raman spectroscopy shows spectral features of Ba-bearing phases, supporting their structural interpretations and close relations with individual later generated silicates.

The probable interpretation of genesis of Ba-rich minerals is supported by a mineral chemistry and textures indicating presence of clay-rich sediments with siliceous components within carbonates where barium is believed to be initially sourced from synsedimentary hydrothermal fluids linked to submarine volcanism. This Ba was probably firstly incorporated into baryte and later remobilised during Variscan and Alpine metamorphism via reactions with silica and clay minerals present in protolith. The transition from detrital to metamorphic minerals allowed Ba to enter feldspars and sheet silicates, depending on pressure-temperature conditions, where barium was preferentially incorporated into feldspars and newly crystallized muscovite during prograde metamorphism. Experimental studies and textural evidence suggest that the most of cymrite formed through hydration of celsian under low-grade metamorphism, consistent with observed mineral stability fields from similar manganese-rich localities associated with Ba-mineralisations. At the Čučma manganese deposit, cymrite is most plausibly interpreted as a product of hydration of celsian, as indicated by its occurrence around corroded celsian grain boundaries. The observed crystal-chemical substitutions in muscovite, especially involving Ba, K, Al, and Si, are shown to play a key role in Ba incorporation mechanisms in studied micas. The Čučma metamorphic manganese deposit offers valuable insights into Ba behaviour during metamorphic evolution in a complex volcanic-sedimentary environment and further depicts the importance of Barich environment for the formation of the final mineral composition of the associating metacarbonates.

Acknowledgements. We want to thank handling editor Jiří Sejkora for his helpful comments. We are also thankful for the reviews of Radek Škoda and one anonymous reviewer for their comments which helped us to improve the manuscript. This work was financially supported by VEGA project (2/0029/23) and APVV-22-0041.

References

ARMBRUSTER T, BERLEPSCH P, GNOS E, HETHERINGTON C J (2002) Crystal chemistry and structure refinments of barian muscovites from the Berisal Complex, Simplon region, Switzerland. Schweiz Mineral Petrogr Mitt 82: 537–547

BAJANÍK Š, VOZÁROVÁ A, HANZEL V, IVANIČKA J, MELLO J, PRISTAŠ J, REICHWALDER P, SNOPKO L, VOZÁR J (1983) Explanations to geological map of the Slovenské rudo-

- horie Mts. Eastern part, 1:50 000. State Geological Institute of Dionýz Štúr, Bratislava, pp 1–223 (in Slovak)
- BERMANEC M, CHUKANOV N V, VARLAMOV D A, RAJAČIĆ A, JANČEV S, ERMOLAEVA V N (2023) Sulfide anomaly related to cymrite–quartz schist of the Kalugeri area, Pelagonian massif, Republic of North Macedonia. J Geo Sci 68(4): 301–311
- Bonatti E, Fisher D E, Joensuu O, Rydell H S, Beyth M (1972) Iron-manganese-barium deposit from the Northern Afar Rift (Ethiopia) Econ Geol 67: 717–730
- CHANG C, Hu W-X, Fu Q, CAO J, WANG X-L, WAN Y, YAO S-P (2018) Characteristics and formation processes of (Ba, K, NH₄)-feldspar and cymrite from a lower Cambrian black shale sequence in Anhui Province, South China. Mineral Mag 82(1): 1–21
- COSTIN G, FAIREY B, TSIKOS H, GUCSIK A (2015) Tokyoite, As-rich Tokyoite, and Noélbensonite: New Occurrences from the Postmasburg Manganese Field, Northern Cape Province, South Africa. Canad Mineral 53(6): 981–990
- COTTERELL T F (2012) The rediscovery of type mineral species at the Benallt manganese mine, Rhiw, Penn Llŷn, Gwynedd, Wales. J Russell Soc 15: 29–40
- DAS GUPTA S P, SEN SARMA R N, DAS GUPTA D R, MARATHE V N (1970) Barian muscovite from the Jhabua manganese belt, Madhya Pradesh, India. Mineral Mag 37(292): 947–950
- ESSENE E J (1967) An occurrence of cymrite in the Franciscan formation, California. Am Mineral 52: 1885–1890
- ESSENE E J, CLAFLIN C L, GIORGETTI G, MATA P M, PEACOR D R, ARKAI P, RATHMELL M A (2005) Two-, three-and four-feldspar assemblages with hyalophane and celsian: implications for phase equilibria in BaAl₂Si₂O₈-CaAl₂Si₂O₈-NaAlSi₃O₈-KAlSi₃O₈. Eur J Mineral 17(4): 515–535
- FARYAD S W (1991) Metamorphosis of the sediments of the early Paleozoic of Gemericum Unit. Miner Slov 23(4): 315–324 (in Slovak)
- Faryad S W (1994) Mineralogy of Mn-rich rocks from greenschist facies sequences of the Gemericum, West Carpathians, Slovakia. Neu Jb Mineral, Mh H 10: 464–480
- FARYAD S W (1995) Determination of the P-T conditions of the metamorphism of the rock complexes of the Spišsko-gemerské rudohorie Mts. Miner Slov 27(1): 9–19 (in Slovak)
- FARYAD S W, ZÁBRANSKÝ F (1996) Newly discovered rockforming minerals of metamophites from the eastern part of the Slovak Ore Mountains. Acta Montan Slovaca 1(2): 131–138 (in Slovak)
- Freeman J J, Wang A, Kuebler K, Jolliff B L, Haskin L A (2008) Characterization of natural feldspars by Raman spectroscopy for future planetary exploration. Canad Mineral 46: 1477–1500
- GRAHAM C M, TAREEN J A K, McMillan P F, Lowe B M (1992) An experimental and thermodynamic study of

- cymrite and celsian stability in the system BaO–Al₂O₃–SiO₂–H₂O. Eur J Mineral 4: 251–269
- Grapes R H (1993) Barian mica and distribution of barium in metacherts and quartzfeldspathic schists, Southern Alps, New Zealand. Mineral Mag 57: 265–272
- GRECULA P (1982) Gemericum a segment of the Paleotethys riftogenic pool. Miner Slov monograph, Bratislava, pp 1–263 (in Slovak)
- Grecula P, Abonyi A, Abonyiová M, Antaš J, Bartalský B, Bartalský J, Dianiška I, Drnzík E, Ďuďa R, Gargulák M, Gazdačko Ľ, Hudáček J, Kobulský J, Lörincz L, Macko J, Návesňák D, Németh Z, Novotný L, Radvanec M, Rojkovič I, Rozložník L, Rozložník O, Varček C, Zlocha J (1995) Mineral deposits of Slovak Ore Mountains. Miner Slov monograph, Bratislava, pp 1–834 (in Slovak)
- Green D I, Cotterell T F, Tindle A G (2019) Barium substitution in muscovite with a comment on ganterite. J Russell Soc 22: 48–58
- HETHERINGTON C J, GIERÉ R, GRASER S (2003) Composition of barium-rich white micas from the Berisal complex, Simplon region, Switzerland. Canad Mineral 41: 1281–1291
- HIRTOPANU P, ANDERSEN J C O, CHUKANOV N, PETRESCU L (2008) Cymrite from Balan sulphide deposit, East Carpathians, Romania, Rocksalt and other nonmetalliferous deposits, Sovata, Romania, 4th–6th Sep 2008, Rom J Mineral Dep 83: 58–61
- Hsu L C (1994) Cymrite: new occurrence and stability. Contrib Mineral Petrol 118: 314–320
- Jakobsen U H (1990) A hydrated barium silicate in unmetamorphosed sedimentary rocks of central North Greenland. Mineral Mag 54: 81–89
- MATSUBARA S, MIYAWAKI R, TIBA T, IMAI H (2000) Tamaite, the Ca-analogue of ganophyllite, from the Shiromaru mine, Okutama, Tokyo, Japan. J Mineral Petrol Sci 95(5): 79–83
- MAZZOLI C, VOZÁROVÁ A (1989) Further data concerning the pressure character of the Hercynian metamorphism in the West Carpathians (Czechoslovakia). Rc Soc Ital Mineral Petrol 43: 635–342
- McSwiggen P L, Morey G B, Cleland J M (1994) Occurrence and genetic-implications of hyalophane in manganese-rich iron-formation, Cuyuna-Iron-Range, Minnesota, USA. Mineral Mag 58: 387–399
- Moles N R (2025) Barian micas and exotic Ba–Cr and Ba–V micas associated with metamorphosed sedimentary exhalative baryte deposits near Aberfedy, Scotland, UK. Minerals 15: 511
- Moro M C, Cembranos M L, Fernandez A (2001) Celsian, (Ba,K)-Feldspar and Cymrite from Sedex Barite Deposits of Zamora, Spain. Canad Mineral 39: 1039–1051
- Myšľan P, Števko M, Mikuš T (2023) Mineralogy and genetic aspects of the metamorphosed manganese

- mineralization at the Július ore occurrence near Betliar (Gemeric Unit, Western Carpathians, Slovakia). J Geosci 68(4): 313–332
- Myšľan P, Števko M, Mikuš T (2024) Mineralogy of metamorphic magnetite—manganese ores at the Prakovce Zimná Voda prospect (Spišsko-gemerské rudohorie Mts., Slovakia): The occurrence of REE-bearing allanite-subgroup minerals ferriakasakaite and ferriallanite. J Geosci 69(4): 231–249
- Myšean P, Števko M, Мікиš T, Vrtiška L (2025a) Mineralogy and genetic considerations of the metamorphosed As-rich manganese ore mineralization at the Diely occurrence near Poráč (Northern Gemeric Unit, Western Carpathians, Slovakia). Mineral Mag 89(1): 71–91
- Myšľan P, Števko M, Sejkora J, Ružička P, Mikuš T (2025b) Metamorphic manganese mineralisation bound to the metacarbonate lenses at the Smolník Malá Hekerová deposit in the Spišsko-gemerské rudohorie Mts., Western Carpathians (Slovakia). Mineral Petrol 119(2): 243–258
- NITSCH K H (1980) Reaction of barium feldspar (celsian) with H₂O to form cymrite under metamorphic conditions. Fortschr Mineral 58, Bh 1: 98–100 (in German)
- Novák M, Škoda R (2007) Mn³+-rich andalusite to kanonaite and their breakdown products from metamanganolite at Kojetice near Třebíč, the Moldanubian Zone, Czech Republic. J Geosci 52: 161–167
- Peterec D, ĎuĎa R (2003) Rare minerals of Mn deposit near Čučma. Natur Carpath 44: 229–236 (in Slovak)
- Peterec D, ĎuĎa R (2009) Manganese mineralization at the locality Čučma. Minerál 17(5): 410–414 (in Slovak)
- Putiš M, Sergeev S, Ondrejka M, Larionov A, Siman P, Spišiak J, Uher P, Paderin I (2008) Cambrian—Ordovician metaigneous rocks associated with Cadomian fragments in the West-Carpathian basement dated by SHRIMP on zircons: A record the Gondwana active margin setting. Geol Carpath 59: 3–18
- RADVANEC M, GONDA S (2020) Succesive formation of Fe and Mn skarns in the Čučma locality (Gemeric unit, W. Carpathians): from metasomatic stage through the amphibolite facies overprint with Ti-rich tephroite to retrograde stilpnomelane—chlorite zone. Miner Slov 52(2): 103–132
- RAITH M, DEVARAJU T, SPIERING, B (2014) Paragenesis and chemical characteristics of the celsian—hyalophane—K-feldspar series and associated Ba—Cr micas in barite-bearing strata of the Mesoarchaean Ghattihosahalli Belt, Western Dharwar Craton, South India. Mineral Petrol 108: 153–176
- REINECKE T (1982) Cymrite and Celsian in Manganese-Rich Metamorphic Rocks from Andros Island/Greece. Contrib Mineral Petrol 79: 333–336
- Rojkovič I (1999) Manganese mineralization in the Western Carpathians, Slovakia. Geol Carpath, special issue 50: 191–192

- Rojkovič I (2000) Mineralogical characteristics of manganese ores in Slovakia. Appendix of the final report Metallogenetic assessment of the territory of the Slovak Republic. Manuscript, ŠGÚDŠ, Bratislava, pp 1–158 (in Slovak)
- ROJKOVIČ I (2001) Early Paleozoic Manganese ores in the Gemericum Superunit, Western Carpathians, Slovakia. Geolines 13: 34–41
- ROMANENKO A V, RASHCHENKO S V, KORSAKOV A V, SOKOL A G (2024) High pressure behaviour of K-cymrite (KAlSi₃O₈·H₂O) crystal structure. Phys Chem Miner 51: 36
- Ružička P, Bačík P, Myšean P, Kurylo S (2020) Grossular and diopside in crystalline limestone from the locality Čučma Čierna baňa (Slovak Republic). Bull Mineral Petrolog 28(1): 94–104
- Ružička P, Myšean P, Števko M, Kurylo S (2021) Atoll garnets in basalt metapyroclastics from the locality Čučma – Vincent (Slovak Republic). Bull Mineral Petrolog 29(1): 16–26 (in Slovak)
- SASSI R, VOZÁROVÁ A (1987) The pressure character of the Hercynian metamorphism in the Gemericum (West Carpathians, Czechoslovakia). Rc Soc Ital Mineral Petrol 42: 73–81
- SEJKORA J, PAULIŠ P, DOLNÍČEK Z, POUR O (2025) Celsian from Chvaletice near Přelouč (Czech Republic). Bull Mineral Petrolog 33(1): 120–127 (in Czech)
- SEKI Y, KENNEDY G C (1964) Phase relations between cymrite, BaAlSi₃O₈(OH) and celsian, BaAl₂Si₂O₈. Am Mineral 49: 1407–1426
- SNOPKOVÁ P, SNOPKO L (1979) Biostratigraphy of the Gelnica series in the Spišsko-gemerské rudohorie Mts. based on palynological results (Western Carpathians, Paleozoic). Západ Karpaty, Sér Geol 5: 57–102 (in Slovak)
- SOROKHTINA N V, CHUKANOV N V, VOLOSHIN A V PAKHOMOVSKY YA A, BOGDANOVA A N, MOISEEV M M (2008) Cymrite as an indicator of high barium activity in the formation of hydrothermal rocks related to carbonatites of the Kola peninsula. Ore Geol Rev 50(7): 620–628
- SOTÁK J, VOZÁROVÁ A, IVANIČKA J (2000) A new microfossils from the Early Paleozoic formations of the Gemericum. Slovak Geol Mag 6 (2–3): 275–277
- ŠONTEVSKA V, JOVANOVSKI G, MAKRESKI P (2007) Minerals from Macedonia. Part XIX. Vibrational spectroscopy as identificational tool for some sheet silicate minerals. J Mol Struct 834: 318–327
- ŠTEVKO M, PLECHÁČEK J, VENCLÍK V, MALÍKOVÁ R (2015) Hausmannite a manganosite from the Čučma – Čierna baňa manganese deposit (Slovak Republic). Bull mineralpetrolog Odd Nár Muz, Praha 23(1): 39–42
- Theye T, Schreyer W, Fransolet A M (1996) Low-temperature, low-pressure metamorphism of Mn-rich rocks in the Lienne Syncline, Venn-Stavelot Massif (Belgian Ardennes) and the role of carpholite. J Petrol 37: 797–783

- Tracy R J (1991) Ba-rich micas from the Franklin Marble, Lime Crest and Sterling Hill, New Jersey. Am Mineral 76: 1683–1693
- Tracy R J, Beard J S (2003) Manganoan kinoshitalite in Mn-rich marble and skarn from Virginia. Am Mineral 88: 740–747
- Vozárová A (1993) Variscan metamorphism and crustal evolution in Gemericum Unit. Západ Karpaty, Ser Mineral Petrogr Geochem Metal 16: 55–117 (in Slovak)
- Vozárová A, Šarinová K, Larionov A, P Resnyakov S, Sergeev S (2010) Late Cambrian/Ordovician magmatic
- arc type volcanism in the Southern Gemericum basement, Western Carpathians, Slovakia: U–Pb (SHRIMP) data from zircons. Int J Earth Sci (Geol Rundsch) 99(1): 17–37
- Vozárová A, Rodionov N, Šarinová K, Presnyakov S (2017) New zircon ages on the Cambrian–Ordovician volcanism of the Southern Gemericum basement (Western Carparthians, Slovakia): SHRIMP dating, geochemistry and provenance. Int J Earth Sci 106: 2147–2170
- WARR LN (2021) IMA-CNMNC approved mineral symbols. Mineral Mag 85: 291–320